Appl Phys B (2009) 94: 51–63
DOI 10.1007/s00340-008-3280-3

Applied Physics B
Lasers and Optics

Measurements of high-pressure CO_2 absorption near 2.0 μm and implications on tunable diode laser sensor design

G.B. Rieker · J.B. Jeffries · R.K. Hanson

Received: 20 March 2008 / Revised version: 24 September 2008 / Published online: 11 November 2008

Abstract A tunable diode laser (TDL) is used to measure the absorption spectra of the R46 through R54 transitions of the 20012 ← 00001 band of CO_2 near 2.0 μm (5000 cm^{-1}) at room temperature and pressures to 10 atm (densities to 9.2 amagat). Spectra are recorded using direct absorption spectroscopy and wavelength modulation spectroscopy with second-harmonic detection (WMS-2f) in a mixture containing 11% CO_2 in air. The direct absorption spectra are influenced by non-Lorentzian effects including finite-duration collisions which perturb far-wing absorption, and an empirical χ-function correction to the Voigt line shape is shown to greatly reduce error in the spectral model. WMS-2f spectra are shown to be at least a factor of four less-influenced by non-Lorentzian effects in this region, making this approach more resistant to errors in the far-wing line shape model and allowing a comparison between the spectral parameters of HITRAN and a new database which includes pressure-induced shift coefficients. The implications of these measurements on practical, high-pressure CO_2 sensor design are discussed.

PACS 33.20.Ea · 42.62.Fi · 07.57.Ty

G.B. Rieker (✉) · J.B. Jeffries · R.K. Hanson
High Temperature Gasdynamics Laboratory, Department of Mechanical Engineering, Stanford University, Building 520, Room 520i, Panama Mall & Duena Street, Stanford, CA 94305, USA
e-mail: grieker@stanfordalumni.org
Fax: +1-650-7231748

J.B. Jeffries
e-mail: jay.jeffries@stanford.edu

R.K. Hanson
e-mail: rkhanson@stanford.edu

1 Introduction

Ever-increasing fuel costs and government regulations on combustion systems continue to drive the development of more efficient combustion devices. As combustion technologies mature, gains in combustion efficiency become more difficult to achieve and accurate diagnostics, often located near the reaction zone of the device, are necessary to evaluate small differences between various device designs. In addition, active control with sensor feedback becomes important to maintain optimum efficiency through transients in system operating points and fuel streams. Since carbon dioxide (CO_2) is a major product of combustion and occurs atmospherically only at very low levels, measurement of CO_2 in a reacting system provides the most direct measure of combustion efficiency. Other combustion technologies, such as gasification in which carbonaceous materials are converted into carbon monoxide and hydrogen, also gain valuable information on the composition of the output gas stream through the monitoring of CO_2. Since many of these combustion devices (internal combustion engines, gas turbine engines, and coal gasifiers) operate at high pressures, the ability to design practical, field-deployable CO_2 sensors capable of accurate measurements at high pressure is increasingly important.

Despite this need, very little work can be found on practical absorption-based measurements of CO_2 at high pressure. Recent field-deployable, absorption-based sensors for *high-pressure* environments have primarily utilized the near-infrared (NIR) spectral region. They employ telecommunications-grade diode lasers using either direct absorption spectroscopy [1–3] or wavelength modulation spectroscopy [4, 5], or NIR hyperspectral sources using direct absorption spectroscopy [6]. The primary advantage to

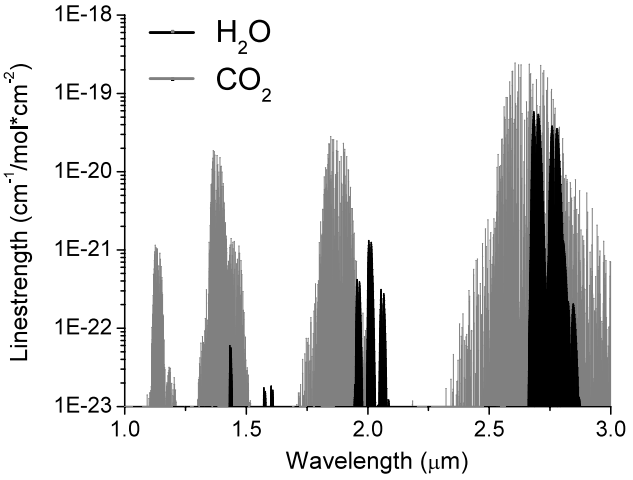

Fig. 1 Linestrengths of H_2O and CO_2 transitions in the near-infrared at 296 K [12]

working in the NIR spectral region is the availability of mature, robust, relatively low-cost laser sources and fiber-optic components developed for the telecommunications industry. These sources and components make compact, portable sensors for accessing real-world environments possible. Figure 1 shows the infrared spectra of H_2O and CO_2 from 1 to 3 μm at 296 K. The bands of CO_2 near 2 μm were chosen for this study because they offer a $10x$–$30x$ improvement in absorption strength over the bands near 1.4 and 1.6 μm while still being accessible with telecommunications-grade, fiber-coupled diode lasers. Recently, for example, a 2.0 μm fiber-coupled diode laser was multiplexed together with several 1.4 μm lasers onto one fiber to make simultaneous measurements of CO_2 and H_2O in a harsh scramjet environment [7]. This example, along with others at 2.0 μm in near-atmospheric environments (e.g., [8–10]), shows the utility of the 2.0 μm region for near-term practical sensor development, particularly until diode lasers at longer wavelengths that access even stronger bands mature [11].

Before a practical high-pressure CO_2 diagnostic near 2.0 μm can be designed for high pressure environments, several important aspects of high-pressure CO_2 absorption must be studied:

(1) Spectral database—Extending sensor capability to high-pressure environments is made difficult by the broadening and overlap of discrete spectral features at high gas density. In lower pressure environments (less than a few atmospheres), the diode laser wavelength can be swept over an entire discrete absorption feature and the pressure-independent absorbance used to infer gas properties (temperature or concentration) knowing only the linestrength and lower state energy of the feature. At high pressures, the blending of adjacent absorption features means that absorption sensors operating in these regimes must rely on comparison between measurements and pressure-dependent spectral simulations to infer gas properties. To achieve accurate results, these simulations must be based on accurate spectral parameters, including pressure broadening and shift. Fortunately, several spectral databases that include the necessary parameters have been compiled which include CO_2 (e.g., [12, 13]), and some comparisons between measurement and simulation have been carried out [14–22]. This paper presents the first comparisons of spectral parameters in the 2.0 μm region at high density, including the important new pressure shift parameters of [13].

(2) Non-Lorentzian effects—Accurate spectral simulations also rely on accurate line shape models for the individual absorption features. Burch et al. performed measurements on the 1.4, 2.7, and 4.3 μm regions of CO_2 [15] and revealed that even at pressures of a few atmospheres, CO_2 absorption spectra exhibit non-ideal behavior. Of primary importance at high gas density is the breakdown of the impact approximation inherent to the Lorentzian line shape profile used to model absorption line shapes in spectral simulations. This approximation assumes that collisions occur instantaneously and neglects energy-level perturbation due to the finite duration of the collision event. The breakdown of the impact approximation causes a reduction in absorption in the far wing (more than a few wavenumbers from line center) compared to that predicted by the Lorentzian line shape. The potentially large errors induced by improper modeling of absorption line shapes at high density will have a direct affect on sensor accuracy.

Several researchers focused on the 4.3 μm region of CO_2, and their measurements at temperatures up to 800 K and pressures up to 60 atm were used to deduce empirical χ-functions to correct for the effects of finite-duration collisions in the far wings of the Lorentzian profile [20, and references therein]. Here, we present the first comparison of measurement and simulation utilizing this empirical correction in the 2.0 μm region of CO_2 absorption to determine the accuracy of this correction in this spectral region.

(3) Absorption measurement strategy—Wavelength modulation spectroscopy with second harmonic detection (WMS-2f) has been shown to exhibit several advantages over direct absorption for harsh, high pressure environments [4, 5], and is therefore a strong candidate for high pressure CO_2 diagnostics. In particular, dividing the WMS-2f signal by the first harmonic (1f) signal normalizes the WMS-2f signal for perturbations in laser intensity [23]. This replaces the need to measure a non-absorbing baseline (as with direct absorption), which is extremely important for harsh, high pressure environments where laser intensity changes rapidly due

to beam perturbations, and a non-absorbing baseline is not present between spectral features due to blending of neighboring transitions. In addition, combining 1f normalization with a spectral model that includes laser-specific tuning parameters [24] eliminates the need for calibration between the model and measurement at a known condition. Most importantly, it was recently suggested that wavelength modulation spectroscopy with second-harmonic detection (WMS-2f) is less influenced by non-Lorentzian effects in high density gases [25]. In the work presented here, both WMS and direct absorption spectra and simulations are compared to show the potential benefits (and drawbacks) of the technique for measuring high pressure CO_2 absorption.

Specifically, we report direct absorption and WMS spectra from the high-frequency edge of the 20012 ← 00001 band of CO_2 between 5005 and 5010 cm^{-1} (~2.0 μm) at room temperature and pressures up to 10 atm (densities up to 9.2 amagat) in a mixture of 10.8% CO_2 in air. This spectral region was chosen because it contains transitions which are useful for combustion measurements (relatively isolated from H_2O vapor and with lower-state energy ~1000 cm^{-1}) [26]. This region is also more generally useful because it is located near the edge of the band, where non-Lorentzian effects are strongest and large lower state energy lines reside. Performing the measurements at 10 atm and room temperature generates a high density gas (equivalent to 40 atm at 1200 K) to particularly highlight non-Lorentzian effects and to decouple the pressure-broadening coefficients and pressure-shift parameters from their temperature exponents. This simplifies interpretation of errors in these coefficients, but further high temperature studies will be needed to confirm the temperature exponents.

The measurements are compared with simulations using the spectral parameters of HITRAN 2004 [12] and Toth et al. [13] and both an unmodified Voigt profile and a Voigt profile modified with the χ-functions in [20]. To the authors' knowledge, we report the first high-density spectra of CO_2 absorption at 2.0 μm, and as such provide a means to test the most recent spectral database and χ-functions, as well as determine the implications on practical sensor design for high-pressure environments.

The paper results in four important conclusions:

(1) Improved agreement between experiment and spectral simulation can be obtained using the recent spectral database of Toth et al. [13].
(2) Even at moderate densities (4.6 amagat, equivalent to 5 atm at room temperature), the breakdown of the impact approximation can have a large effect on spectral simulations of direct absorption spectra of CO_2 in the 2.0 μm region.
(3) The χ-function corrections of Perrin and Hartmann [20] for non-Lorentzian line shape effects due to the breakdown of the impact approximation reduce error between experiment and spectral simulation for direct absorption.
(4) The WMS-2f spectra are minimally affected by the breakdown of the impact approximation and the factors which lead to this difference are discussed.

Overall, the work presented in this paper represents an important step in developing first-generation absorption-based high pressure CO_2 diagnostics by revealing the important considerations which must be addressed during diagnostic design.

2 Absorption spectroscopy

2.1 Direct absorption spectroscopy

The simplest form of absorption spectroscopy is direct absorption spectroscopy in which monochromatic light (such as from a laser) is passed through the test gas region to a detector and the attenuation of the light is quantified by the Beer–Lambert relation:

$$\left(\frac{I_t}{I_o}\right)_v = \exp\left\{-\sum_j S_j(T)\cdot\phi_j(T,P,x_i,x_{k\neq i},v) \times P\cdot x_i\cdot L\right\}. \quad (1)$$

Here, I_o and I_t are the incident and transmitted intensity at optical frequency v, respectively. P is the total system pressure, T is the temperature, x_i is the mole fraction of the absorbing gas, $x_{k\neq i}$ are the mole fractions of all other species in the mixture, and L is the absorbing pathlength over which the light has traveled. The collection of terms in brackets is referred to as the absorbance. It contains the linestrength, S, and the line shape function, ϕ, of the transition j. The line shape function, which will be discussed further in Sect. 2.3, contains several more transition-dependent spectral parameters such as line-broadening coefficients and pressure-induced shift coefficients. The linestrength and line shape functions are summed over all transitions to account for the overlap of neighboring spectral transitions due to broadening.

The spectral parameters (S, line-broadening coefficients, pressure-induced shift coefficients, etc.) for many molecules have been studied and catalogued into databases, such as HITRAN 2004 [12], making it possible to use the Beer–Lambert relation to simulate spectra for a variety of gas conditions. An unknown gas property (T, x_i, or P) can be inferred by comparing the measured light attenuation at one

wavelength with simulated spectra as a function of the unknown property. Multiple unknown gas properties can be determined using the attenuation at multiple suitably-chosen wavelengths.

Direct absorption spectroscopy becomes difficult in high-density environments when the zero-absorption 'baseline' between distinct spectral features becomes obscured by the broadened and blended wings of adjacent features. The baseline is necessary to determine the incident laser intensity (I_o), which can be changing with time due to laser power drift, window fouling, beam steering, and scattering. Thus in high-density environments, direct absorption spectroscopy must rely on differential absorption techniques [27], the use of a separate non-resonant laser at a spectrally-distant wavelength to track the baseline [2], or a stable measurement environment in which the incident laser intensity is not changing and a pre- or post-experiment measure of laser intensity can be performed.

2.2 Wavelength modulation spectroscopy

Wavelength modulation spectroscopy with second-harmonic detection (WMS-2f) is similar to direct absorption spectroscopy, except the laser wavelength is rapidly modulated and the resulting detector signal is passed through a lock-in amplifier to isolate only the frequency components of the detector signal near the second harmonic of the modulation frequency. Like direct absorption, the WMS-2f signal is dependent on spectral parameters and gas properties and can therefore be compared with spectral simulations to infer gas properties. However, WMS-2f has several benefits which make it desirable over direct absorption for certain sensing applications.

The WMS-2f signal is sensitive to spectral shape or curvature rather than absolute absorption levels, which is useful for certain high-density spectra [28], particularly those that are affected by the breakdown of the impact approximation [25]. The use of a lock-in amplifier serves to reject noise that falls outside the pass band, such as laser intensity and electronic noise. For injection current-tuned diode lasers, there is a simultaneous modulation of the laser wavelength and intensity. This intensity modulation is typically the strongest component of the WMS-1f signal, which can be obtained by passing the detector signal through a lock-in tuned to the first harmonic of the modulation frequency. The WMS-1f signal is proportional to the incident laser intensity and therefore can be used to normalize the WMS-2f signal against perturbations to the laser intensity by laser drift, window fouling, beam steering, or scattering [23, 29].

There is extensive coverage in the literature on models for WMS (e.g., [30–32]). More recently, it has been shown that the use of 1f-normalization and inclusion of laser-specific tuning parameters into the WMS simulation models enable calibration-free measurements (where scaling of the temperature and concentration measurement from a known condition is no longer necessary) [5, 7, 24, 25].

It should be noted that there are several drawbacks to WMS. Signal interpretation is more difficult since the model is more complex than the Beer–Lambert relation and includes assumptions that one must ensure are appropriate for the experiment. In addition, the WMS-1f signal can be affected by absorption, which means an estimate of the nominal conditions within the test gas is necessary to reduce error in the WMS-1f model when using 1f-normalized WMS-2f to infer unknown properties in environments with large absorbance [7]. Note that for the work presented here, all properties of the test gas are known, so the contribution of absorption to the WMS-1f signal is included directly in the model.

A more complete treatment of the model for 1f-normalized, WMS-2f for injection current-tuned diode lasers with large modulation amplitude and real laser tuning characteristics can be found in the literature [24]. Here, the model which is used for the WMS simulations throughout this work is summarized. The WMS-2f signal is described by

$$R_{2f} = \frac{G\bar{I}_o}{2}\Bigg[\Bigg(H_2 + \frac{i_o}{2}(H_1 + H_3)\cos\psi_1 + i_2\Bigg(H_o + \frac{H_4}{2}\Bigg)\cos\psi_2\Bigg)^2 + \Bigg(\frac{i_o}{2}(H_1 - H_3)\sin\psi_1 + i_2\Bigg(H_o - \frac{H_4}{2}\Bigg)\sin\psi_2\Bigg)^2\Bigg]^{1/2}, \quad (2)$$

where G is the optical-electrical gain of the detector, $\bar{I}_o$ is the average laser intensity, and i_o and i_2 represent the linear and first term of the nonlinear intensity modulation amplitude, normalized by $\bar{I}_o$ [24]. The terms ψ_1 and ψ_2 represent the phase shift between the intensity modulation and frequency (wavelength) modulation. Though higher-order nonlinear terms are present with many diode lasers, for the particular lasers and modulation amplitudes used in this study, they can be neglected. The use of the symbol R conforms with the convention of [24] and denotes that the so-called zero-absorption background (which is caused by the nonlinear intensity modulation) is still contained in (2). In practice, this background (which is constant over time) is vector subtracted from both the simulation and the measurement before direct comparison [7].

The WMS-1f signal is typically dominated by the injection current modulation of the laser intensity, and is given by

$$R_{1f} = \frac{G\bar{I}_o}{2}\Bigg[\Bigg(H_1 + i_o\Bigg(H_o + \frac{H_2}{2}\Bigg)\cos\psi_1 + \frac{i_2}{2}(H_1 + H_2)\cos\psi_2\Bigg)^2$$

Table 1 Expressions for χ-functions [20]. $\Delta\nu$ is the frequency de-tuning from line center. σ_i are de-tuning cutoff frequencies in cm^{-1}

$\lvert\Delta\nu\rvert$ (cm^{-1})		$\chi(\Delta\nu, T)$
CO_2–CO_2	CO_2–N_2	
$0 < \lvert\Delta\nu\rvert < \sigma_1 = 3$	$0 < \lvert\Delta\nu\rvert < \sigma_1 = 3$	1
$\sigma_1 < \lvert\Delta\nu\rvert < \sigma_2 = 30$	$\sigma_1 < \lvert\Delta\nu\rvert < \sigma_2 = 10$	$\exp[-B_1 \times (\lvert\Delta\nu\rvert - \sigma_1)]$
$\sigma_1 < \lvert\Delta\nu\rvert < \sigma_2 = 120$	$\sigma_1 < \lvert\Delta\nu\rvert < \sigma_2 = 70$	$\exp[-B_1 \times (\sigma_2 - \sigma_1) - B_2 \times (\lvert\Delta\nu\rvert - \sigma_2)]$
$\lvert\Delta\nu\rvert > \sigma_3$	$\lvert\Delta\nu\rvert > \sigma_3$	$\exp[-B_1 \times (\sigma_2 - \sigma_1) - B_2 \times (\sigma_3 - \sigma_2) - B_3 \times (\lvert\Delta\nu\rvert - \sigma_3)]$

$$+\left(i_o\left(H_o - \frac{H_2}{2}\right)\sin\psi_1 + \frac{i_2}{2}(H_1 - H_3)\sin\psi_2\right)^2\Bigg]^{1/2}. \quad (3)$$

The H_k terms can be represented by

$$H_0(T, P_i, \bar{v}, a) = \frac{1}{2\pi}\int_{-\pi}^{\pi}\exp\left\{-\sum_j S_j(T)\cdot\phi_j(T, P, x, \bar{v} + a\cos\theta)\cdot P\cdot x_i\cdot L\right\}d\theta, \quad (4)$$

$$H_k(T, P_i, \bar{v}, a) = \frac{1}{\pi}\int_{-\pi}^{\pi}\exp\left\{-\sum_j S_j(T)\cdot\phi_j(T, P, x, \bar{v} + a\cos\theta)\cdot P\cdot x_i\cdot L\right\}\cos k\theta\, d\theta, \quad (5)$$

where $\bar{v}$ is the average laser optical frequency and a is the amplitude of the frequency (wavelength) modulation. These H terms do not make any assumption about optical thickness and can be used for all conditions.

2.3 Line shape model

The Lorentzian line shape profile is traditionally used to describe pressure-broadened spectral transitions. This line shape profile makes use of the impact approximation, which assumes that collisions occur instantaneously. It has been shown that the impact approximation breaks down in the far-wing region (beyond a few wavenumbers from line center) due to the increased importance of the finite duration of collisions on the energy levels of molecules that contribute to far-wing absorption [14–22]. As shown by Winters et al. [14] and later by Burch et al. [15], this effect is manifest by lower measured absorbance in the far-wings of CO_2 features than is predicted by the traditional Lorentzian profile.

As density increases, collisional-broadening shifts a larger portion of the integrated absorbance of a spectral transition to the far-wing region. Thus the effect of the breakdown in the impact approximation becomes more prominent at higher densities. Several researchers developed empirical corrections to the Lorentzian profile based on low-temperature (193–296 K), near-atmospheric data in the 4.3 μm region [16–19]. These corrections are applied through a frequency-dependent χ-function that is multiplied with the line shape function of individual absorption features. Perrin and Hartmann [20] coupled the data of [16–19] with their own data at 4.3 μm in gases up to 60 atm and 800 K to develop a temperature- and frequency-dependent χ-function for CO_2–CO_2 and CO_2–N_2 collisions. This model was used by Scutaru et al. [21] at elevated temperatures (<800 K) and low pressures (<1 atm) for the 4.3 and 2.7 μm region. Good agreement was found at 4.3 μm; however, the χ-functions had very little effect for the particular spectra and conditions used for the 2.7 μm data and thus provided little useful information on accuracy there. The model was tested in the 2.3 μm window region by Tonkov et al. [22] for pure CO_2 at high pressure (to 50 atm) and room temperature. They found that the χ-functions under-predicted the absorption and proposed new factors. These researchers believe that the largest influence in the 2.3 μm region is the bands in the 2.7 μm region and that the new factors likely also account for several local effects which influence the window region (weak allowed bands, collision-induced absorption, etc.). Theoretical approaches based on first-principles calculations have been proposed first for CO_2 broadened by simple perturbers (e.g., Argon) [33, 34] and later for self-broadened CO_2 [35]; however, these approaches require large computing resources and to our knowledge are not yet applicable to CO_2–N_2 mixtures.

The model of Perrin and Hartmann [20] was chosen for this work because it contains the most recent formulation for CO_2–N_2 mixtures. The analytical expressions for the χ-functions used in this work are shown in Table 1. The temperature-dependence of the χ-functions is introduced through the analytical law for calculating B_1, B_2, and B_3:

$$B_i(T) = \alpha_i + \beta_i\exp(-\varepsilon_i T),$$

where the coefficients α, β, and ε are found in Table 2.

Table 2 Parameters for temperature-dependent terms in χ-function calculations [20]

	CO_2–CO_2				CO_2–N_2		
	α	β	ε		α	β	ε
B_1	0.0888	−0.160	0.00410	B_1	0.416	−0.354	0.00386
B_2	0	0.0526	0.00152	B_2	0.00167	0.0421	0.00248
B_3	0.0232	0	0	B_3	0.0200	0	0

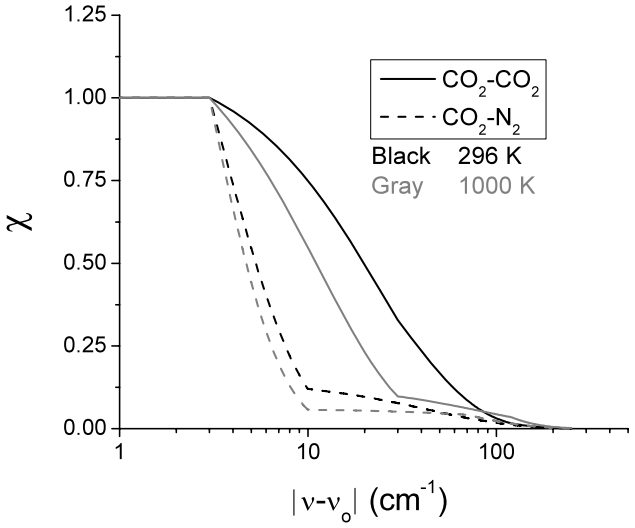

Fig. 2 CO_2–CO_2 and CO_2–N_2 χ-functions versus frequency de-tuning from line center [20]

Figure 2 is a plot of the χ-functions versus frequency de-tuning from line center for CO_2–CO_2 collisions and CO_2–N_2 collisions at 296 K. When the χ-functions are multiplied with the Voigt line shape profile, the effect is to reduce the overall line shape function in the far-wings of individual features.

2.4 Spectroscopic data

In addition to a good line shape model, measurements in high-pressure environments require an accurate database of spectroscopic parameters. HITRAN 2004 [12] is a large compilation of calculated and measured spectral parameters for many species. In terms of CO_2, HITRAN 2004 includes line positions, strengths, lower-state energies, and broadening parameters; however, it does not include pressure-induced shift coefficients. Recently, Toth et al. performed an extensive experimental survey of CO_2 absorption from 4500–7000 cm^{-1} [36–38]. The measurements and modeling include line position and strength [36], self-broadening and self-induced pressure shift coefficients [37], and air-broadening and air-induced pressure shift coefficients [38]. The Toth studies have been compiled into a database [13]. The linestrength coefficients of Toth et al. are within 3%

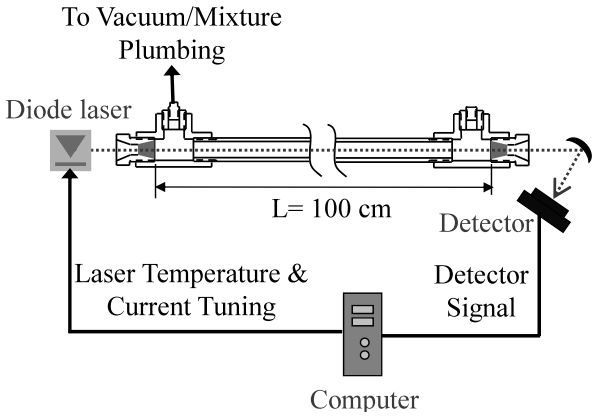

Fig. 3 Experimental setup with high-pressure static cell

and the self-broadening coefficients are within 6.8% of low pressure measurements in the 5005–5010 cm^{-1} region by Webber et al. [26]. The Toth et al. coefficients are also in general agreement with linestrength, broadening, and pressure shift measurements at low pressure by Corsi et al. [39] in the 4990–5005 cm^{-1} region. Of significant importance, however, is that the new pressure shift parameters of Toth et al. and the broadening coefficients of both HITRAN 2004 and Toth et al. have not been tested in the 2.0 μm region against measurements at more than 1 atm.

3 Experimental method

3.1 Experimental setup

A schematic of the experimental setup is shown in Fig. 3. Light from a fiber-coupled diode laser emitting near 1.997 μm (5008 cm^{-1}, NEL America Inc.) is passed to a fiber-collimator (Thorlabs F220FC-1550 nm) and sent through the test cell. Despite being well outside the optimal wavelength range specified for the collimator, an acceptably small divergence angle is achieved to maintain a relatively small beam diameter across the 100 cm length of the test cell. A spherical mirror collects the beam onto a room temperature extended-InGaAs detector (New Focus, 700 kHz bandwidth). The detector signal is sent through a low-pass analog filter before digital sampling by a multifunction data acquisition card (National Instruments 6115,

12-bit A/D conversion) in a desktop PC. The signal is stored and later post-processed using a software lock-in amplifier to recover the WMS-2f and WMS-1f signals. The laser modulation is provided by the same PC and multifunction card.

The static optical cell is stainless steel with interchangeable body sections to form different pathlengths (100 cm was used here). Sapphire windows with 1 cm open aperture are epoxied in the cell end caps. The surfaces of the window through which the beam passes have a 1° wedge to avoid creating an etalon within or between the windows. A vacuum system and mixture tank are connected via stainless manifold. Temperature is measured with three type K thermocouples and pressure is determined with 1000 or 10000 Torr Baratron capacitance manometers.

3.2 Experimental procedure

To obtain the spectra shown in Sect. 4 and 5, the average injection current of the diode laser is held constant (with rapid current modulation superimposed for WMS) and the laser thermoelectric cooler (TEC) is used to vary the laser temperature, thereby tuning the average laser wavelength across the spectral region of interest. The laser control and data acquisition process is automated using Labview and a GPIB controller in communication with the laser controller. The optical cell is first filled with pure, dry air to the desired experimental pressure. The incident laser intensity (I_o in (1)) for the direct absorption spectra and the zero-absorption background for the WMS spectra are acquired by running the automated program once with the cell filled with this non-absorbing medium. As mentioned in Sect. 2.2, the WMS background due to laser nonlinearity is subtracted from both the measurement and simulation before direct comparison. The program tunes the laser to a temperature setpoint, waits 2 minutes to be sure the laser has completely stabilized and then acquires 5 seconds of the detector signal. The rapid modulation is turned on for WMS, the laser is again allowed to stabilize for 2 minutes, and the detector signal is acquired for 5 seconds. The modulation is turned off, the laser is moved to the next temperature setpoint, and the process is repeated for each data point. The cell is then evacuated and filled with the CO_2/air mixture to the desired experimental pressure, and the process repeated to obtain the transmitted laser intensity (I_t in (1)) for the direct absorption spectra and the absorbing WMS signal.

Prior to and after the completion of data collection, the automated process was repeated with the WMS modulation off and the laser output directed to a wavemeter to obtain the calibration between laser temperature setpoint and wavelength. Unlike the results reported for a similar process using NIR diode lasers near 1.4 μm for high-pressure measurements of H_2O [25], this particular diode laser exhibited negligible wavelength shift due to modulation (i.e., less than the 0.005 cm^{-1} wavelength uncertainty of the measurement). This may be due in part to the internal temperature stabilization properties of this laser and the lower modulation depth used for these measurements. All WMS spectra reported in this paper use modulation depth $a = 0.11$ cm^{-1} and modulation frequency $f = 50$ kHz (characterized with a Ge etalon with 0.016 cm^{-1} free spectral range). Note that the WMS-2f signal at a given spectral feature peak is maximized for a modulation amplitude that is 2.2 times the half-width at half-max of the spectral feature [30]. For the 10 atm spectra presented here, a modulation amplitude of ~1.5 cm^{-1} would be necessary to maximize the 2f signal, which is not obtainable with the current laser due to injection current limitations.

Also note that the experimental technique presented here was developed in order to obtain high quality spectra over a 5 cm^{-1} region with a tunable diode laser to achieve the goals set forth in the introduction. In a practical sensor implementation for harsh environments with fast transients, the average wavelength of one of more lasers would be fixed or injection-current scanned over a short range of suitably-chosen locations to achieve the desired measurement bandwidth (up to 100 kHz has been achieved with this technique [40]).

4 Direct absorption results

In this section, the direct absorption spectra are presented and compared with simulations using the database of Toth et al. [13] with (1) an unmodified Voigt line shape profile and (2) a Voigt line shape profile modified by the χ-functions of Perrin and Hartmann [20]. The Voigt profile was chosen over the Lorentzian profile for accuracy at lower pressures; however, even at 1 atm the Voigt profile is dominated by the Lorentzian component. Figure 4 shows the experimental results plotted with the simulations. The measured spectra, represented by the black squares, covers the R46 through R54 lines of the 20012 ← 00001 band of $^{12}C^{16}O_2$ centered at 4978.6 cm^{-1}. The step size of the measured spectra was chosen to be 0.1 cm^{-1}, which represents a good trade-off between resolution and acquisition time for each spectrum. The signal to noise ratio is such that measurement uncertainty bars would fall within the data markers, and measurement uncertainty is further reduced through the acquisition of 5 s of data at each point. The largest experimental uncertainty is the mixture CO_2 mole fraction, which is estimated to be ±3%. The dashed lines represent the simulations using only the Voigt profile and the solid lines denote the simulations which include the χ-functions. At 1 atm the difference between the simulations is negligible; however, as pressure increases, the rising difference illustrates the influence of the far-wings of the stronger features to the red of the measured

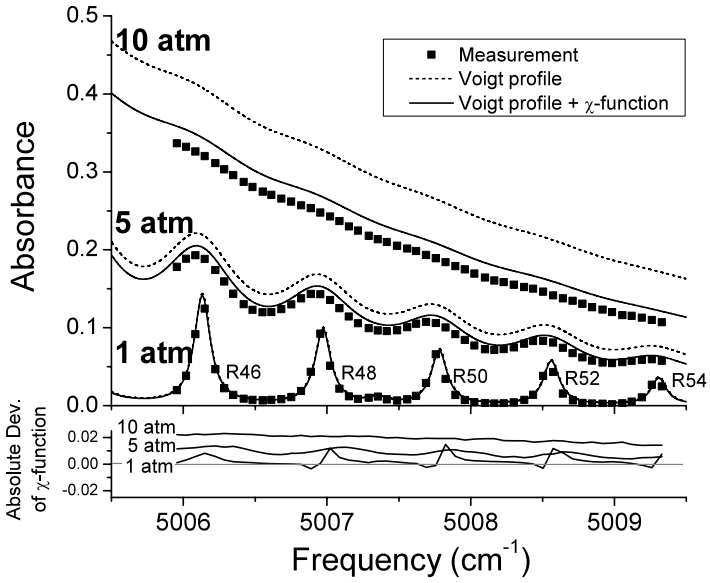

Fig. 4 Direct absorption spectrum, 10.8% CO_2 in air, $L = 100$ cm, $T = 296$ K. Absolute deviation is shown for the Voigt profile + χ-function data

spectra. The average error in this region is reduced by application of the χ-function from 24% to 8.5% for the 5 atm spectrum and from 40% to 10% for the 10 atm spectrum.

The remaining error is the result of several factors. The Perrin and Hartmann χ-functions were developed with data from the 4.3 μm region of CO_2 [16–20]. The measurements of Burch et al. [15] on the 4.3, 2.7, and 1.4 μm regions of CO_2 show that the influence of finite-duration collisions on the Lorentzian line shape decreases with wavelength for the various bands. This would suggest that the χ-function developed at 4.3 μm should under-predict the absorption measured at 2.0 μm. Also, the Perrin and Hartmann χ-functions were developed using the GEISA database,[1] and though they were tested and gave good agreement with the HITRAN 86 database, many updates have been made to this database in the years since and it is somewhat different than the Toth database used here. Finally, the χ-functions of Perrin and Hartmann do not include super-Lorentzian corrections in the intermediate-wing of the absorption feature, which result in enhanced absorption over that predicted by the Lorentzian profile. These corrections are important near absorption bands where effects such as line mixing "transfer intensity from regions of weak absorption to those of strong absorption" [20], and help correct for the fact that the integral of the line shape with the χ-functions of [20] included does not result in unity. An example of enhanced absorption is shown in [25], where super-Lorentzian behavior is reported and accounted for using the χ-functions for H_2O developed by Clough et al. [41], which include super-Lorentzian effects.

[1]GEISA, Laboratoire de Météorologie Dynamique du CNRS, Ecole Polytechnique, Palaiseau 91128, France.

The simulated absorbance with and without the χ-function for the entire 20012 ← 00001 band is shown in Fig. 5 with the measurement region for Fig. 4 demarcated. One can see the measurement region is near the edge of the band. It is therefore hypothesized that the slight overprediction of absorbance in this region by the χ-function with respect to the measured data in Fig. 4 is the compound result of under-prediction of super-Lorentzian effects in the intermediate-wings of nearby features and over-prediction of sub-Lorentzian effects due to finite-duration collisions.

5 WMS-2f results

The WMS results are shown in Figs. 6, 7, 8 for 1, 5, and 10 atm, respectively. At 1 atm, good agreement is obtained between simulation and experiment and the non-Lorentzian effects result in an average difference of only 0.3% compared to an unmodified Voigt profile. For the 5 atm case (4.6 amagat), good agreement is obtained and again the χ-function shows little effect on the simulated spectra (0.8%). At 10 atm (9.2 amagat), the effect of χ-function corrections to the line shape becomes apparent in the simulated spectrum (6.3%).

Table 3 summarizes the effect of non-Lorentzian behavior on the WMS and direct absorption signals at all pressures. The percentage differences in Table 3 were calculated by taking the difference between the simulations with and without the χ-function and comparing with the χ-function corrected case. The reported result is the average for the region between 5005.5 and 5009.5 cm^{-1}. One can immediately see that the WMS signals are much less affected by non-Lorentzian behavior than direct absorption. The WMS-2f signal is sensitive to curvature in the absorption spectrum,

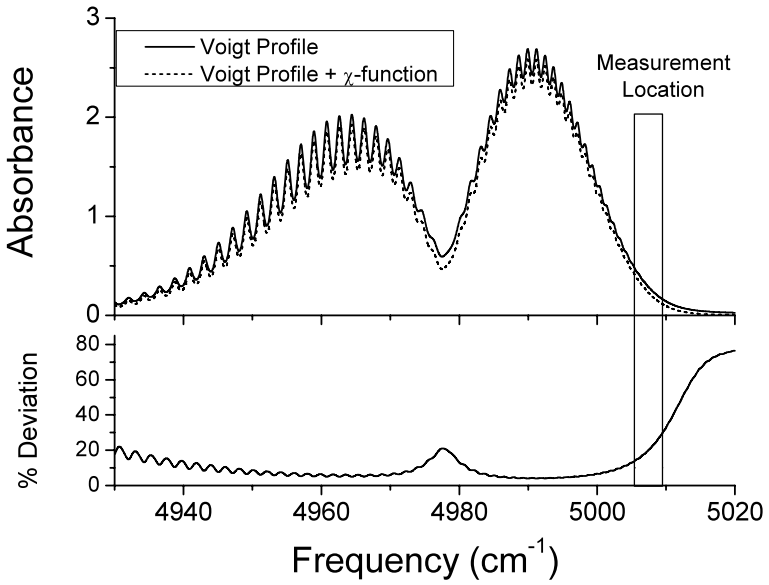

Fig. 5 Simulated direct absorption spectrum of the 20012 ← 00001 band of CO_2 near 2.0 μm. The box denotes the measurement region for this work. 10.8% CO_2 in air, $P = 10$ atm, $L = 100$ cm, $T = 296$ K

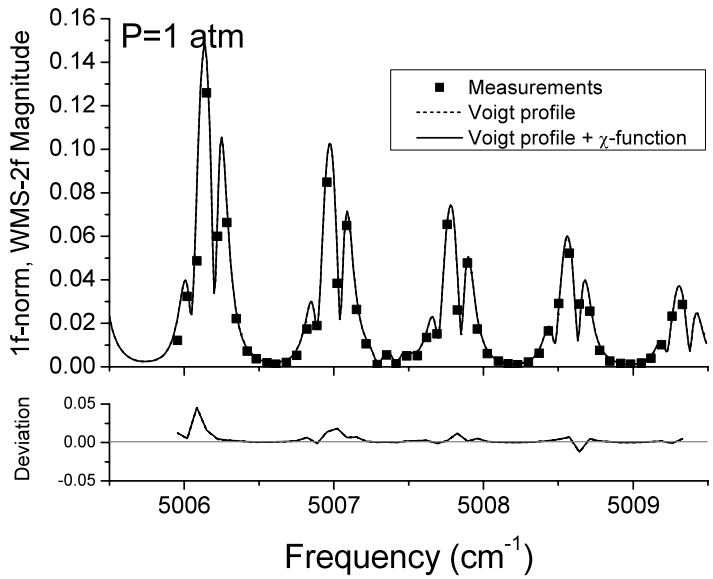

Fig. 6 1f-normalized, WMS-2f spectrum. $P = 1$ atm, 10.8% CO_2 in air, $L = 100$ cm, $T = 296$ K, $a = 0.11$ cm^{-1}. χ-function correction results in nearly identical spectra

and therefore the difference in the WMS-2f signal between the simulations arises from slight variation in the curvature of the spectrum due to the non-Lorentzian effects. The difference in the influence of the non-Lorentzian effects on the direct absorption and WMS-1f signals is due to the different dependences on absolute absorption between the two. The direct absorption signal is the absorbance, so if, for example, the absorbance at 5007.5 cm^{-1} is modeled as 28.2% for the unmodified Voigt and 22.4% for the χ-function modified Voigt, the direct absorption signal experiences a 26% effect due to non-Lorentzian effects. The WMS-1f signal is approximately proportional to (1-*absorbance*). Therefore, for the same example above, we expect the WMS-1f signal to change by ∼7.5% due to non-Lorentzian effects. Indeed, the actual simulations show that it changes by 5.7%.

A quantitative comparison between spectral databases cannot be carried out with direct absorption spectra at high pressures because the effect of non-Lorentzian behavior is large and the χ-function corrections carry large uncertainty. We have shown here and in [25] that the use of WMS reduces the effects of non-Lorentzian behavior, so even though there are larger uncertainties in the WMS models than in the Beer–Lambert relation for direct absorption, WMS provides a method to make accurate comparisons between spectral databases at high pressures. Figure 9 shows the WMS data at 5 and 10 atm with simulations using the Toth database and the HITRAN 2004 database with a χ-function modified Voigt profile. The comparison shows that both databases give accurate values for the linestrengths and broadening coefficients at room temperature; however, the

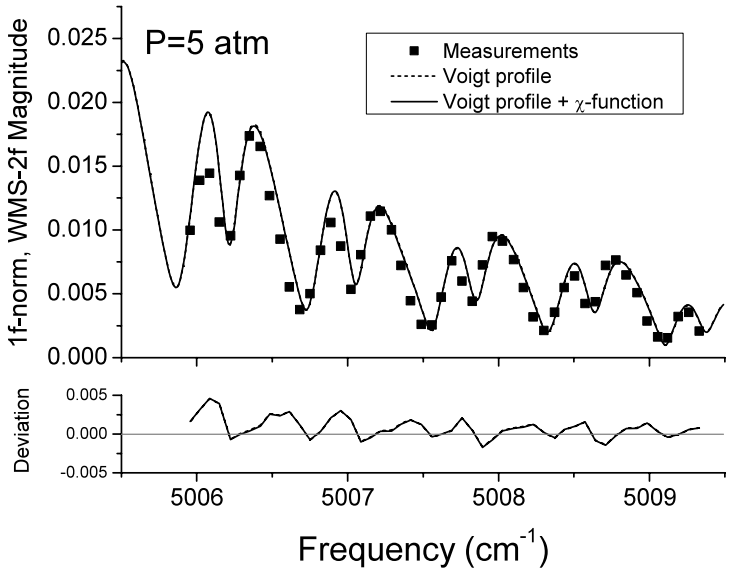

Fig. 7 1f-normalized, WMS-2f spectrum. $P = 5$ atm, 10.8% CO_2 in air, $L = 100$ cm, $T = 296$ K, $a = 0.11$ cm^{-1}. χ-function correction results in nearly identical spectra

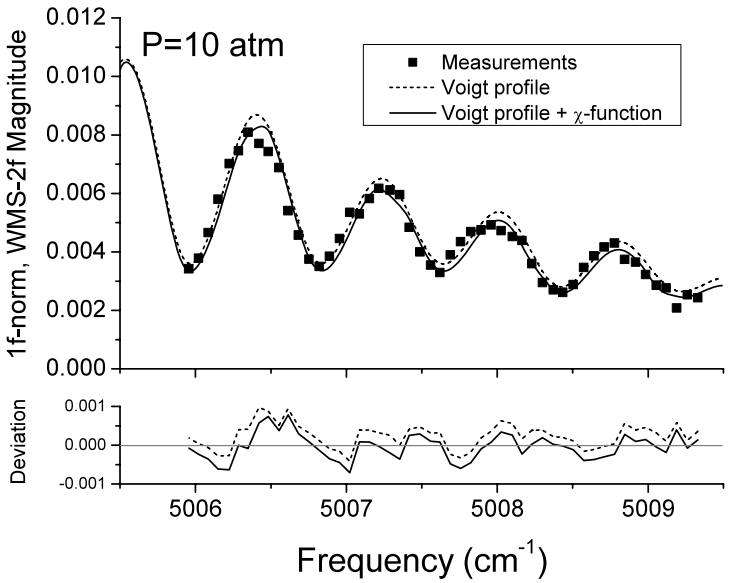

Fig. 8 1f-normalized, WMS-2f spectrum. $P = 10$ atm, 10.8% CO_2 in air, $L = 100$ cm, $T = 296$ K, $a = 0.11$ cm^{-1}

Table 3 The average effect of non-Lorentzian behavior on WMS and direct absorption signals in the 5005.5–5009.5 cm^{-1} region

	Average % effect of non-Lorentzian behaviour on signal*		
	1 atm	5 atm	10 atm
WMS-2f	0.3	1.5	4.6
WMS-1f	0.1	1.5	5.7
1f-norm, WMS-2f	0.3	0.8	6.3
Direct absorption	6.7	13.8	27.1

*With respect to χ-function corrected signal

lack of pressure-induced shift coefficients in the HITRAN 2004 database induces significant error in the simulations. A slight frequency shift between the experiment and the simulations using the pressure shift parameters of Toth et al. is apparent (and perhaps easier to see in Figs. 7 and 8). Analysis reveals that augmenting the average pressure-induced shift coefficients of Toth et al. by -0.004 cm^{-1}/atm provides improved agreement at all pressures. This falls outside the reported uncertainty of the pressure shift coefficients in Toth et al. [37, 38]; however, one should note that shift co-

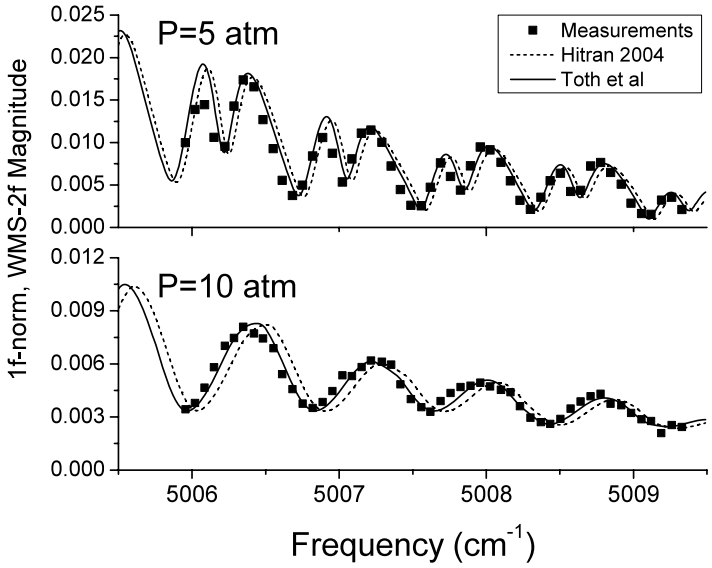

Fig. 9 Comparison of simulations using HITRAN 04 [12] and Toth et al. [13] spectral parameters. 1f-normalized, WMS-2f at $T = 296$ K, 10.8% CO_2 in air, $L = 100$ cm. Both simulated spectra use the χ-function modified Voigt profile

efficients are very difficult to accurately measure at the low pressures employed for spectral validations, and often uncertainties for spectral parameters are calculated from fitting uncertainties, which do not take systematic error into account.

6 Implications on sensor design for high pressures

Direct absorption and 1f-normalized WMS-2f spectra were reported for the R46 through R54 lines of the 20012 ← 00001 band of CO_2 near 2.0 μm at room temperature and up to 10 atm. The measurements have several important implications to guide future absorption-based sensor design for high pressure CO_2 measurements:

(1) Spectral parameters—The WMS spectra show that the recently-measured spectral parameters of Toth et al. [13] improve upon those found in HITRAN 2004, primarily due to the inclusion of pressure-induced shift coefficients. These parameters should be chosen over HITRAN 04 for the simulations needed to infer gas parameters from measurements at high pressure. The slight discrepancy that remains between measurements and simulations likely results from remaining errors in the line-shift parameters. Augmenting line-shift parameters by -0.004 cm^{-1}/atm provides improved agreement in the 5005–5010 cm^{-1} region.

(2) Non-Lorentzian effects—The direct absorption spectra show that non-Lorentzian effects at high gas densities pose an important challenge to CO_2 sensor design, particularly toward the edge of absorption bands where one finds the large lower-state energy transitions that are useful for measurements in high temperature environments. The temperature- and frequency-dependent χ-functions of Perrin and Hartmann [20] were used to model the non-Lorentzian behavior and reduced the average error from 24% to 8.5% at 5 atm (4.6 amagat) and 40% to 10% at 10 atm (9.2 amagat). The remaining error is likely due to the lack of inclusion of intermediate-wing super-Lorentzian effects in the χ-function model and the fact that the model was developed for the 4.3 μm region of CO_2. The applicability of the χ-functions closer to the band center is still an open question. Thus, an easy-to-implement, well-validated model for non-Lorentzian effects on high pressure CO_2 absorption in the 2.0 μm region still does not exist that delivers the low uncertainty levels necessary for accurate inference of gas properties using direct absorption spectroscopy. An alternate approach is for the sensor designer to look to techniques which reduce the influence of non-Lorentzian effects on the final uncertainty of the measurement.

(3) Absorption measurement strategy—The 1f-normalized WMS-2f spectra are shown to be significantly less influenced by non-Lorentzian effects than the direct absorption spectra. The average effect of the non-Lorentzian behavior in this region at 10 atm is 6% for the WMS spectra compared with 27% for the direct absorption spectra. This is a very important benefit of WMS at high gas densities because it reduces reliance on line shape correction for non-Lorentzian effects. The reduced influence of non-Lorentzian effects also implies that the WMS signals experience reduced influence by the far-wings of distant spectral features, thus reducing the size of the spectral region around the wavelengths used for the sensor for which an accurate spectral database is necessary.

An additional advantage of WMS injection current-tuned diode lasers at high pressures is the ability to use the 1f signal as a 'baseline' to track perturbations to the laser intensity (window fouling, beam-steering, etc.). Direct absorption-based sensors do not have a direct means to account for this once the non-absorbing baseline between spectral features is obscured by the wings of pressure-broadened features.

The disadvantages of WMS need also be considered when choosing a technique for high-pressure sensing. First, there are more assumptions in the current WMS models than in the simple Beer–Lambert relation for direct absorption (truncated higher-order laser nonlinearities, linear wavelength modulation, etc.) and the model relies on measurements of the laser-specific tuning characteristics. These assumptions introduce the possibility for error depending on the experimental conditions. Second, from Figs. 6, 7, 8, one can see that the peak WMS signal is reduced by nearly a factor of 20 from 1 to 10 atm, while the direct absorption signal grows with pressure. This decrease in signal is caused by the reduction in curvature of the absorption spectrum, which will continue to diminish at higher densities. The high-pressure signal loss can be counteracted by increasing the wavelength modulation amplitude [28]; however, the modulation amplitude is eventually limited by the modulation current limits of a given diode laser. Third, since WMS is dependent on the curvature of the absorption spectrum, it also is more sensitive to near-wing lineshape (i.e., broadening parameters). Finally, using WMS to infer gas properties in environments with greater than a few percent absorption requires an estimate of concentration to nominally account for absorption in the WMS-1f signal [7].

Overall, 1f-normalized WMS-2f is a good candidate for sensing in high-pressure environments when sufficient spectral curvature is present to support an acceptable signal-to-noise ratio. When density is increased such that sufficient signal is not achievable with the highest modulation depth possible for the diode laser, another technique which is resistant to the influence of non-Lorentzian line shape behavior should be explored, such as differential absorption [27].

This work represents an important step toward near-term practical, field-deployable sensor systems for measuring CO_2 in high-pressure environments. The next step in the development process is to select specific wavelengths at which to 'fix' the laser, apply the sensor to a simultaneously high temperature and pressure environment, and determine a method to account for water vapor interference.

Acknowledgements This work was supported by the Electric Power Research Institute with Dr. R. Steele as technical monitor and the Air Force Office of Scientific Research (AFOSR) with Dr. J. Tishkoff as technical monitor.

References

1. S.T. Sanders, J.A. Baldwin, T.P. Jenkins, D.S. Baer, R.K. Hanson, Proc. Combust. Inst. **28**, 587–594 (2000)
2. D.W. Mattison, J.B. Jeffries, R.K. Hanson, R.R. Steeper, S. De Zilwa, J.E. Dec, M. Sjoberg, W. Hwang, Proc. Combust. Inst. **31**, 791–798 (2007)
3. E. Schlosser, T. Fernholz, H. Teichert, V. Ebert, Spectrochim. Acta **58**, 2347–2359 (2002)
4. T. Fernholtz, H. Teichert, V. Ebert, Appl. Phys B **75**, 229–236 (2002)
5. G.B. Rieker, H. Li, X. Liu, J.T.C. Liu, J.B. Jeffries, R.K. Hanson, M.G. Allen, S.D. Wehe, P.A. Mulhall, H.S. Kindle, A. Kakuho, K.R. Sholes, T. Matsuura, S. Takatani, Proc. Combust. Inst. **31**, 3041–3049 (2007)
6. L.A. Kranendonk, J.W. Walewski, T. Kim, S.T. Sanders, Proc. Combust. Inst. **30**, 1619–1627 (2005)
7. G.B. Rieker, J.B. Jeffries, R.K. Hanson, Calibration-free wavelength modulation spectroscopy for harsh, non-uniform environments. Appl. Opt. (2008, submitted)
8. P. Werle, K. Maurer, R. Kormann, R. Mücke, F. D'Amato, T. Lancia, A. Popov, Spectrochim. Acta **58**, 2361–2372 (2002)
9. L. Sandström, S. Bäckström, H. Ahlberg, S. Höjer, A.G. Larsson, Infrared Phys. Technol. **39**, 69–75 (1998)
10. M.E. Webber, R. Claps, F.V. Englich, F.K. Tittel, J.B. Jeffries, R.K. Hanson, Appl. Opt. **40**, 4395–4403 (2001)
11. A. Farooq, J.B. Jeffries, R.K. Hanson, Appl. Phys. B **90**, 619–628 (2008)
12. L.S. Rothman, D. Jacquemart, A. Barbe, D.C. Benner, M. Birk, L.R. Brown, M.R. Carleer, C. Chackerian Jr., K. Chance, L.H. Coudert, V. Dana, V.M. Devi, J.-M. Flaud, R.R. Gamache, A. Goldman, J.M. Hartmann, K.W. Jucks, A.G. Maki, J.-Y. Mandin, S.T. Massie, J. Orphal, A. Perrin, C.P. Rinsland, M.A.H. Smith, J. Tennyson, R.N. Tolchenov, R.A. Toth, J.V. Auwera, P. Varanasi, G. Wagner, J. Quant. Spectrosc. Radiat. Transfer **96**, 139–204 (2005)
13. R.A. Toth, L.R. Brown, C.E. Miller, V.M. Devi, D.C. Benner, J. Quant. Spectrosc. Radiat. Transfer **109**, 906–921 (2008)
14. B.H. Winters, S. Silverman, W.S. Benedict, J. Quant. Spectrosc. Radiat. Transfer **4**, 527 (1964)
15. D.E. Burch, D.A. Gryvnak, R.R. Patty, C.E. Bartky, J. Opt. Soc. Am. **59**, 267 (1969)
16. R. Le Doucen, C. Cousin, C. Boulet, A. Henry, Appl. Opt. **24**, 897 (1985)
17. V. Menoux, R. Le Doucen, C. Boulet, Appl. Opt. **26**, 554 (1987)
18. C. Cousin-Lucasseau, Absorption I.R. du CO_2 dans la fenêtre atmosphérique autor de 4.2 μm-détermination de la dépendance en température du coefficient d'absorption. Influence des interférences spectrales sur le profil abservé. Thesis, Rennes (1987)
19. R. Le Doucen, C. Cousin, C. Boulet, A. Henry, Appl. Opt. **24**, 3899 (1985)
20. M.Y. Perrin, J.M. Hartmann, J. Quant. Spectrosc. Radiat. Transfer **42**, 311–317 (1989)
21. D. Scutaru, L. Rosenmann, J. Taine, R.B. Wattson, L.S. Rothman, J. Quant. Spectrosc. Radiat. Transfer **50**, 179–191 (1993)
22. M.V. Tonkov, N.N. Filippov, V.V. Bertsev, J.P. Bouanich, N. Van-Thanh, C. Brodbeck, J.M. Hartmann, C. Boulet, F. Thibault, R. Le Doucen, Appl. Opt. **35**, 4863–4870 (1996)
23. D.T. Cassidy, J. Reid, Appl. Opt. **21**, 1185–1190 (1982)
24. H. Li, G.B. Rieker, X. Liu, J.B. Jeffries, R.K. Hanson, Appl. Opt. **45**, 1052–1061 (2006)
25. G.B. Rieker, X. Liu, H. Li, J.B. Jeffries, R.K. Hanson, Appl. Phys. B **87**, 169–178 (2007)
26. M.E. Webber, S. Kim, S.T. Sanders, D.S. Baer, R.K. Hanson, Y. Ikeda, Appl. Opt. **40**, 821–828 (2001)
27. A.E. Klingbeil, J.B. Jeffries, R.K. Hanson, Proc. Combust. Inst. **31**, 807–815 (2007)

28. J.T.C. Liu, J.B. Jeffries, R.K. Hanson, Appl. Opt. **43**, 6500–6509 (2004)
29. R.T. Wainner, B.D. Green, M.G. Allen, M.A. White, J. Stafford-Evans, R. Naper, Appl. Phys. B **75**, 249–254 (2002)
30. J. Reid, D. Labrie, Appl. Phys. B **26**, 203 (1981)
31. J. Silver, Appl. Opt. **31**, 707–717 (1992)
32. P. Kluczynski, O. Axner, Appl. Opt. **38**, 5803–5815 (1999)
33. J. Boissoles, V. Menoux, R. Le Doucen, C. Boulet, D. Robert, J. Chem. Phys. **91**, 2163–2171 (1989)
34. Q. Ma, R.H. Tipping, C. Boulet, J. Chem. Phys. **104**, 9678–9688 (1996)
35. Q. Ma, R.H. Tipping, C. Boulet, J. Bouanich, Appl. Opt. **38**, 599–604 (1999)
36. R.A. Toth, L.R. Brown, C.E. Miller, V.M. Devi, D.C. Benner, J. Mol. Spectrosc. **239**, 229–242 (2006)
37. R.A. Toth, L.R. Brown, C.E. Miller, V.M. Devi, D.C. Benner, J. Mol. Spectrosc. **239**, 243–271 (2006)
38. R.A. Toth, L.R. Brown, C.E. Miller, V.M. Devi, D.C. Benner, J. Mol. Spectrosc. **242**,131–157 (2007)
39. C. Corsi, F. D'Amato, M. De Rosa, G. Modugno, Eur. Phys. J. D **6**, 327–332 (1999)
40. H. Li, A. Farooq, J.B. Jeffries, R.K. Hanson, Appl. Phys. B **89**, 407–416 (2007)
41. S.A. Clough, F.X. Kneizys, R.W. Davies, Atmos. Res. **23**, 229–241 (1989)